LINEAR STABILITY ANALYSIS OF OPEN-CHANNEL SHEAR FLOW GENERATED BY VEGETATION

Adriano C. de Lima[1], Norihiro Izumi[2]

ABSTRACT

A linear stability analysis of flow in an open-channel partially covered with vegetation was performed. The differential drag between vegetated zones and adjacent non-vegetated zones is known to induce a lateral gradient of the streamwise velocity. The velocity gradient may result in flow instability in the shear layer around the edge of the vegetated zone, causing the generation of discrete horizontal vortices. We assume that the base state flow field before the occurrence of instability is characterized by turbulence, with a smaller length scale than the flow depth, which is mainly generated by the bottom friction. By introducing perturbations to the flow depth as well as the streamwise and transverse velocities in the base state, the conditions required for perturbations grow in time were studied over a wide range of (1) Froude number, (2) normalized non-vegetated zone width, and three other dimensionless parameters which represent the relative effect of (3) bed

[1]Division of Field Engineering for the Environment, Graduate School of Engineering, Hokkaido University, Sapporo, Japan, 0608628. E-mail: adriano@eng.hokudai.ac.jp.

[2]Division of Field Engineering for the Environment, Graduate School of Engineering, Hokkaido University, Sapporo, Japan, 0608628. E-mail: nizumi@eng.hokudai.ac.jp.

friction, (4) vegetation drag and (5) sub-depth eddy viscosity. All parameters were found to have positive and negative growth rates of perturbations within their respective evaluated ranges. The characteristic vortex shedding frequencies associated with the maximum growth rate was compared with those observed in experiments. Although the analysis which employs a base state set without the large scale lateral motions was shown to be capable of predicting the order of magnitude of the frequencies, there is a systematic discrepancy between the predicted and observed frequencies which may be due to the limitation of linear stability analysis.

Keywords: Linear stability analysis, shear flow, flow instability, kinematic eddy viscosity, lateral vortices.

INTRODUCTION

The presence of vegetation is commonly observed in both natural and rectified watercourses. Vegetation in watercourses is desirable in some cases as it prevents bank erosion and provides habitat and food for numerous species. On the other hand, vegetation causes serious problems in other cases as it increases channel resistance and reduces channel capacity for the draining of flood water. Vegetation in a part of a channel produces transverse shear flow, which may lead to flow instability and the generation of large-scale horizontal vortices. These horizontal vortices have a strong influence on the velocity distribution and the amount of discharge conveyed by a channel without overflow, and enhance the lateral mixing of not only the flow itself, but also the substances transported by the flow both inside and outside the vegetated area. Therefore, it is important to determine the conditions under which instability occurs, and the characteristics of the horizontal vortices from both an engineering and an environmental points of view. Though various studies on instability in channels with lateral velocity gradients have been performed, only theoretical studies on instability in vegetated or compound channels are reviewed herein.

Tamai et al. (1986) observed the generation of large eddies on the water surface in a set of experiments with compound channels consisting of a main channel and a flood plain. They concluded that the shear layer in the lateral velocity profile around the interface between the main channel and the flood plain is the predominant cause for the generation of large eddies. They applied the stability analysis of Michalke (1964) with the use of the Rayleigh stability equation to their experimental results, and found that their observations were able to be explained by the analysis.

Chu et al. (1991) performed a linear stability analysis of shear flows in channels with varying flow depths and varying bottom roughness. They employed the St. Venant shallow water equations with the free water surface approximated by a rigid lid, which is a valid simplification when the Froude number is close to zero. The perturbation equations reduced to a modified Rayleigh equation, which can be relatively easily solved. Because it is not possible to reproduce the lateral gradient of the streamwise velocity without including the Reynolds stress in their formulation, they adopted an assumption that the flow depth and the bottom roughness vary gradually across the channel in order to approximate it. They found that flow stabilizes when the bottom roughness is sufficiently large, and the lateral variation of flow is sufficiently small.

Ikeda et al. (1994) performed a temporal linear stability analysis of a partially vegetated channel. They obtained the base state flow with the use of the St. Venant shallow water equations including the Reynolds stress expressed by the lateral kinematic eddy viscosity empirically determined in experiments. In the perturbed problem, however, they ignored the Reynolds stress and the variation of the water surface elevation, in effect reducing their perturbed equations to a modified Rayleigh equation again. They found that the dimensional angular frequency of maximum instability is uniquely correlated with the ratio of two velocities a sufficient distance from the boundary between the non-vegetated and vegetated zones.

Ghidaoui and Kolyshkin (1999) performed a temporal linear stability analysis of a channel flow with lateral velocity gradients without the rigid-lid assumption. The Reynolds stress was included in their formulation by means of the eddy viscosity term of Chen and Jirka (1997). Semi-empirical expressions were used to describe the base flow profile, containing regression parameters which were not correlated to a specific flow field (i.e., the source of flow retardation in part of the channel was not specified). Their computations showed that the influence of the Reynolds number, defined using the eddy viscosity, on the stability domain is small when it surpasses 1000.

Prooijen and Uijttewaal (2002) have also included the turbulent viscosity as in Chen and Jirka (1997) in their temporal and spatial linear stability analysis of a channel flow with a lateral velocity gradient generated by two separate water supplies with different velocities. The mean flow field, which varied along the streamwise direction, was assumed to be the base state and the rigid-lid assumption was employed, which is a reasonable simplification, given that the Froude number in their experimental runs did not exceed 0.5.

White and Nepf (2007) performed a complete set of experiments and a spatial stability analysis of a channel partially obstructed by an array of circular cylinders by the use of the modified Rayleigh equations following Chu et al. (1991), with the Reynolds stress scaled with the width of the shear layer around the edge of the array. They made use of the rigid-lid assumption, in accordance with the condition of small Froude numbers met in their experiments (always below 0.25). They concluded that even though the drag differential due to the vegetation reinforces the shear instability, the overall drag damps it if the background friction in the channel is sufficiently large.

In this study, we perform a temporal linear stability analysis of flow in an open channel partially covered with vegetation. By not employing the rigid-lid and the inviscid flow assumptions, we could study the effects of the Froude number and the kinematic eddy viscosity, respectively, on the growth rate of perturbations. We employ the St. Venant shallow water equations with the Reynolds stress included to reproduce the velocity gradient due to the differential drag between the regions with and without vegetation. The temporal and spatial variations of the flow vanish except for the lateral variation of the streamwise velocity in the base state, which is used as a starting point of the stability analysis. This base state flow field is not, however, simply a temporal average of the flow affected by fully-developed horizontal vortices, but the flow undisturbed by the vortices. We thus employ a kinematic eddy viscosity representing turbulence with a length scale smaller than the flow depth. Differently from Chen and Jirka (1997), the eddy viscosity employed herein is estimated for the flow unaffected by the large-scale horizontal vortices. We impose perturbations on the base state flow velocities and flow depth, and study how various hydraulic parameters affect the time development of the perturbations.

FORMULATION

Suppose that water is flowing through a wide rectangular open-channel with lateral emergent rigid vegetation (trees) as shown in Fig. 1. The vegetation is modeled by an array of regularly spaced cylinders with a uniform diameter installed only on one side of the channel. The model of cylinders as vegetation employed herein has been widely used in previous studies (e.g., Ikeda et al. (1994), Tsujimoto and Kitamura (1992), White and Nepf (2007) and Xiaohui and Li (2002)). The region of the channel covered with vegetation is defined as the 'vegetated zone', the width of which is denoted by $\tilde{B}_v$. The region of the channel without vegetation is defined as the 'non-vegetated zone', the width of which is denoted by $\tilde{B}$.

Governing equations

In this study, we focus on horizontal vortices generated in shallow flow in a wide rectangular open channel. The horizontal length scale of the vortices is commonly large compared with the length scale of flow depth. The generation of such thin vortices can be described by the depth-averaged shallow water formulation. In particular, the momentum equations employed in this analysis need to include the Reynolds stress and the drag force due to vegetation in order to represent the lateral velocity distribution due to the differential drag between the non-vegetated and vegetated zones. The momentum equations in the streamwise and transverse directions ($\tilde{x}$ and $\tilde{y}$) and the continuity equation are

$$\frac{\partial \tilde{U}}{\partial \tilde{t}} + \tilde{U}\frac{\partial \tilde{U}}{\partial \tilde{x}} + \tilde{V}\frac{\partial \tilde{U}}{\partial \tilde{y}} = gS - g\frac{\partial \tilde{H}}{\partial \tilde{x}} - \frac{\tilde{T}_{bx} + \tilde{D}_x}{\rho \tilde{H}} + \frac{1}{\rho}\left(\frac{\partial \tilde{T}_{xx}}{\partial \tilde{x}} + \frac{\partial \tilde{T}_{xy}}{\partial \tilde{y}}\right), \tag{1a}$$

$$\frac{\partial \tilde{V}}{\partial \tilde{t}} + \tilde{U}\frac{\partial \tilde{V}}{\partial \tilde{x}} + \tilde{V}\frac{\partial \tilde{V}}{\partial \tilde{y}} = -g\frac{\partial \tilde{H}}{\partial \tilde{y}} - \frac{\tilde{T}_{by} + \tilde{D}_y}{\rho \tilde{H}} + \frac{1}{\rho}\left(\frac{\partial \tilde{T}_{yx}}{\partial \tilde{x}} + \frac{\partial \tilde{T}_{yy}}{\partial \tilde{y}}\right), \tag{1b}$$

$$\frac{\partial \tilde{H}}{\partial \tilde{t}} + \frac{\partial \tilde{U}\tilde{H}}{\partial \tilde{x}} + \frac{\partial \tilde{V}\tilde{H}}{\partial \tilde{y}} = 0, \tag{1c}$$

where $\tilde{t}$ is time, $\tilde{x}$ is the streamwise coordinate, $\tilde{y}$ is the lateral coordinate the origin of which is taken at the interface between the vegetated and non-vegetated zones, $\tilde{U}$ and $\tilde{V}$ are the $\tilde{x}$ and $\tilde{y}$ components of the flow velocity respectively, $\tilde{H}$ is the flow depth, $\tilde{T}_{bx}$ and $\tilde{T}_{by}$ are the $\tilde{x}$ and $\tilde{y}$

components of the bed shear stress respectively, $\tilde{D}_x$ and $\tilde{D}_y$ are the $\tilde{x}$ and $\tilde{y}$ components of the drag force due to vegetation respectively, $\tilde{T}_{ij}$ $(i, j = x, y)$ is the Reynolds stress tensor, ρ is the density of water, g is the gravity acceleration, and S is the bed slope of the channel. The tilde denotes dimensional variables, which is to be dropped after normalization.

The drag force vector ($\tilde{D}_x$, $\tilde{D}_y$) is described by the expression

$$(\tilde{D}_x, \tilde{D}_y) = \begin{cases} 0 & \text{in the non-vegetated zone,} \\ \dfrac{\rho C_D \tilde{a} \tilde{H}}{2} (\tilde{U}^2 + \tilde{V}^2)^{1/2} (\tilde{U}, \tilde{V}) & \text{in the vegetated zone,} \end{cases} \tag{2}$$

where C_D is the drag coefficient of vegetation, typically estimated to range from 1 to 2. In addition, $\tilde{a}$ is a parameter describing the density of vegetation, written by

$$\tilde{a} = \frac{\tilde{d}}{2\tilde{l}_x \tilde{l}_y}, \tag{3}$$

where $\tilde{d}$ is the diameter of cylinders and $\tilde{l}_x$ and $\tilde{l}_y$ are the distances between two adjacent cylinders in the $\tilde{x}$ and $\tilde{y}$ directions respectively, as shown in Fig. 2.

The bed shear stress is related to the flow velocity by means of the bed friction coefficient C_f, such that

$$(\tilde{T}_{bx}, \tilde{T}_{by}) = \rho C_f (\tilde{U}^2 + \tilde{V}^2)^{1/2} (\tilde{U}, \tilde{V}). \tag{4}$$

Though the bed friction coefficient C_f is a weak function of the flow depth relative to the roughness height, it is assumed to be constant and common in both vegetated and non-vegetated zones for simplicity.

With the use of Boussinesq's kinematic eddy viscosity, the Reynolds stresses are expressed by

$$\tilde{T}_{xx} = 2\rho\tilde{\nu}_T \frac{\partial \tilde{U}}{\partial \tilde{x}}, \tag{5a}$$

$$\tilde{T}_{xy} = \tilde{T}_{yx} = \rho\tilde{\nu}_T \left(\frac{\partial \tilde{U}}{\partial \tilde{y}} + \frac{\partial \tilde{V}}{\partial \tilde{x}} \right), \tag{5b}$$

$$\tilde{T}_{yy} = 2\rho\tilde{\nu}_T \frac{\partial \tilde{V}}{\partial \tilde{y}}, \tag{5c}$$

where $\tilde{\nu}_T$ is the kinematic eddy viscosity. We assume that, in the base state before instability occurs, the flow is already affected by turbulence, the length scale of which is smaller than the flow depth (sub-depth scale turbulence). Where there is no influence of vegetation, the kinematic eddy viscosity $\tilde{\nu}_T$ should correspond to the sub-depth scale turbulence generated by the bottom friction. We employ the logarithmic velocity distribution as a sub-depth scale turbulent velocity distribution due to the bottom friction. The kinematic eddy viscosity then takes a parabolic form, which is depth-averaged from the bottom to the water surface, yielding

$$\tilde{\nu}_T = \frac{1}{6}\kappa \tilde{U}_{f\infty} \tilde{H}_\infty, \tag{6}$$

where $\tilde{U}_{f\infty}$ and $\tilde{H}_\infty$ are the friction velocity and the flow depth in the region sufficiently far from the vegetated zone, respectively, and κ is the Kármán constant ($= 0.4$). We assume that the sub-depth scale turbulence is rather isotropic. Therefore, the above formulation is expected to describe the Reynolds stresses in the streamwise and lateral directions a sufficient distance from the vegetated zone. Although the kinematic eddy viscosity in the horizontal direction is known to be larger than in (6), as in Chen and Jirka (1997) where $\tilde{\nu}_T = 0.2\tilde{U}_{f\infty}\tilde{H}_\infty$, we assumed that the increase in the kinematic eddy viscosity is caused by large-scale horizontal vortices generated by instability.

In the shear layer formed around the boundary between the two zones, and inside the vegetated zone, the velocity and the shear velocity are reduced because of the Reynolds stress and the drag force due to vegetation. In addition, the length scale of sub-depth scale vortices may be affected by a typical length scale of vegetation such as the vegetation spacing. According to the experimental results of Ikeda et al. (1991), however, the depth-averaged kinematic eddy viscosity even in the shear layer and the vegetated zone can be represented by (6). This may be attributed to the fact that the sum of the resistant forces (the bed shear stress, the Reynolds stress and the vegetation drag force) remains constant regardless of the reduction in the bed shear stress in the shear layer and the vegetated zone. The kinematic eddy viscosity may be correlated to the total resistant force. Furthermore, since the flow depth and the spacing of vegetation in Ikeda et al.'s experiments are both in the same range, the kinematic eddy viscosity in the vegetated zone may not be strongly affected by vegetation. These assumptions and (6) are employed in this study as well. Therefore, the Reynolds stresses in (1a-b) are expressed by the constant sub-depth kinematic eddy viscosity as in (6), for both the non-vegetated and vegetated zones.

At the side walls, the velocity vanishes in the directions both tangential and normal to the side walls. The following conditions therefore hold:

$$\tilde{U} = 0 \qquad \text{at} \qquad \tilde{y} = \tilde{B}, -\tilde{B}_v, \tag{7a}$$

$$\tilde{V} = 0 \qquad \text{at} \qquad \tilde{y} = \tilde{B}, -\tilde{B}_v. \tag{7b}$$

In the shallow water formulation, however, it is not easy to make use of the conditions of vanishing streamwise velocity (7a) (non-slip conditions). In place of these conditions, the following slip conditions are often used:

$$\frac{\partial \tilde{U}}{\partial \tilde{y}} = 0 \quad \text{at} \quad \tilde{y} = \tilde{B}, -\tilde{B}_v. \tag{8}$$

At a sufficient distance from the boundary between the two zones, the streamwise velocity asymptotically approaches constant velocities in both the non-vegetated and vegetated zones in the base state. If $\tilde{B}$ and $\tilde{B}_v$ are sufficiently large, and the slip condition (8) holds, the streamwise velocity is constant at both side walls in the base state, i.e. for which

$$\tilde{U} = \tilde{U}_\infty \quad \text{at} \quad \tilde{y} = \tilde{B}; \quad \tilde{U} = \tilde{U}_{-\infty} \quad \text{at} \quad \tilde{y} = -\tilde{B}_v, \tag{9}$$

where $\tilde{U}_\infty$ and $\tilde{U}_{-\infty}$ are the velocities at a sufficient distance from the boundary in the non-vegetated and vegetated zones, respectively. We assume that both side walls are located at a sufficient distance from the boundary, and employ (7b) and (8) as the boundary conditions at the side walls.

Right at the boundary between the non-vegetated and vegetated zones, the velocities, flow depth and shear stresses are continuous, such that

$$\lim_{\tilde{y}\to+0} \left(\tilde{U}, \tilde{V}, \tilde{H}, \tilde{T}_{xx}, \tilde{T}_{xy}, \tilde{T}_{yy}\right) = \lim_{\tilde{y}\to-0} \left(\tilde{U}, \tilde{V}, \tilde{H}, \tilde{T}_{xx}, \tilde{T}_{xy}, \tilde{T}_{yy}\right). \tag{10}$$

Normalization

At a sufficient distance from the boundary between the two zones in the base state normal flow equilibrium condition, $\tilde{U}$ and $\tilde{H}$ are constant, and $\tilde{V}$ vanishes. Thus, (1) allows the solutions

$$\tilde{U}_\infty = \left(\frac{g\tilde{H}_\infty S}{C_f}\right)^{1/2}, \quad \tilde{U}_{-\infty} = \left(\frac{2g\tilde{H}_\infty S}{2C_f + C_D\tilde{a}\tilde{H}_\infty}\right)^{1/2}. \tag{11}$$

The velocity and flow depth at a sufficient distance from the vegetated zone, $\tilde{U}_\infty$ and $\tilde{H}_\infty$ are used for the normalization. The velocities and flow depth are then rendered dimensionless according to the following expressions:

$$(\tilde{U}, \tilde{V}) = \tilde{U}_\infty (U, V), \quad \tilde{H} = \tilde{H}_\infty H. \tag{12}$$

The independent variables $\tilde{x}$, $\tilde{y}$ and $\tilde{t}$ are normalized with the use of the width of the non-vegetated zone $\tilde{B}$, such that

$$(\tilde{x}, \tilde{y}) = \tilde{B}(x, y), \quad \tilde{t} = \frac{\tilde{B}}{\tilde{U}_\infty} t. \tag{13}$$

With the use of the above normalization, the governing equations (1) are rewritten in the form

$$\frac{\partial U}{\partial t} + U\frac{\partial U}{\partial x} + V\frac{\partial U}{\partial y} = -F^{-2}\frac{\partial H}{\partial x} + \beta\left(1 - \frac{T_{bx} + D_x}{H}\right) + \epsilon\left(\frac{\partial^2 U}{\partial x^2} + \frac{\partial^2 U}{\partial y^2}\right), \tag{14a}$$

$$\frac{\partial V}{\partial t} + U\frac{\partial V}{\partial x} + V\frac{\partial V}{\partial y} = -F^{-2}\frac{\partial H}{\partial y} - \beta\frac{T_{by} + D_y}{H} + \epsilon\left(\frac{\partial^2 V}{\partial x^2} + \frac{\partial^2 V}{\partial y^2}\right), \tag{14b}$$

$$\frac{\partial H}{\partial t} + \frac{\partial UH}{\partial x} + \frac{\partial VH}{\partial y} = 0, \tag{14c}$$

where (T_{bx}, T_{by}) and (D_x, D_y) are the normalized bed shear stress and vegetation drag vectors, respectively, written in the form

$$(T_{bx}, T_{by}) = \left(U^2 + V^2\right)^{1/2} (U, V), \tag{15a}$$

$$(D_x, D_y) = \begin{cases} \alpha \left(U^2 + V^2\right)^{1/2} H\,(U, V) & \text{if} \quad -B_v \leq y \leq 0, \\ 0 & \text{if} \quad 0 \leq y \leq 1. \end{cases} \tag{15b}$$

The above normalized governing equations include the four non-dimensional parameters β, ϵ, F and α. The parameter β, which expresses the relative importance of the bed shear effect, is dependent on the aspect ratio of the non-vegetated zone $A_R = \tilde{B}/\tilde{H}_\infty$, and the bottom friction coefficient C_f, such that

$$\beta = \frac{C_f \tilde{B}}{\tilde{H}_\infty} = C_f A_R. \tag{16}$$

The parameter ϵ is associated with the eddy viscosity $\tilde{\nu}_T$, expressed by (6), in the form

$$\epsilon = \frac{\tilde{\nu}_T}{\tilde{U}_\infty \tilde{B}} = \frac{C_f^{1/2} \tilde{H}_\infty}{15 \tilde{B}} = \frac{C_f^{1/2}}{15 A_R}. \tag{17}$$

The Froude number $\tilde{F}$ is given by

$$F = \frac{\tilde{U}_\infty}{\sqrt{\tilde{g} \tilde{H}_\infty}} = \left(\frac{S}{C_f}\right)^{1/2}. \tag{18}$$

The parameter α is related to the vegetation drag and density, and is defined by

$$\alpha = \frac{C_D \tilde{a} \tilde{H}_\infty}{2C_f}. \tag{19}$$

BASE STATE NORMAL FLOW

The base state is set considering the fluid motion before the instabilities take place at the shear layer. Taking the average flow field as the base flow, or introducing a kinematic eddy viscosity including the effect of the vortices would result in a base state which is affected by the perturbations due to the transverse mixing.

In the base state, (14a) reduces to

$$\beta\left(1 - U_0^2\right) + \epsilon \frac{\mathrm{d}^2 U_0}{\mathrm{d}y^2} = 0 \qquad \text{if} \qquad 0 \le y \le 1, \tag{20a}$$

$$\beta\left[1 - U_0^2\left(1+\alpha\right)\right] + \epsilon \frac{\mathrm{d}^2 U_0}{\mathrm{d}y^2} = 0 \qquad \text{if} \qquad -B_v \le y \le 0, \tag{20b}$$

where U_0 is the streamwise velocity in the base state, which is a function only of the transverse coordinate y.

The normalization of ($\tilde{U}_\infty$, $\tilde{U}_{-\infty}$) leads to (1, ϕ), where ϕ is the ratio between the undisturbed velocities in the vegetated and non-vegetated zones at a sufficient distance from their boundary, which is related to the non-dimensional parameter α, such that

$$\phi = \frac{\tilde{U}_{-\infty}}{\tilde{U}_{\infty}} = \frac{1}{(1+\alpha)^{1/2}}. \tag{21}$$

The domain of ϕ is $0 < \phi \leq 1$; ϕ approaches to 0 when vegetation obstructs the flow completely in the vegetated zone ($\alpha \to \infty$), and takes a value of unity when there is no vegetation ($\alpha = 0$).

In the base state, the matching conditions (10) reduce to

$$\lim_{y\to+0} U_0 = \lim_{y\to-0} U_0 = \psi, \quad \lim_{y\to+0} \frac{\mathrm{d}U_0}{\mathrm{d}y} = \lim_{y\to-0} \frac{\mathrm{d}U_0}{\mathrm{d}y}. \tag{22}$$

There is a discontinuity in $\mathrm{d}^2U_0/\mathrm{d}y^2$ at $y = 0$. The velocity between the two zones ψ has a relation with ϕ as

$$\psi = \left(\frac{2\phi^2}{1+\phi}\right)^{1/3}. \tag{23}$$

The above expression was determined from the integration of (20a-b) with respect to y and the introduction of boundary conditions $U_0 = (\phi, 1)$ at $y = (-B_v, 1)$ and matching conditions (22).

Solving (20a,b) under the above referred conditions, we obtain the explicit analytical solutions for U_0 in the form

$$U_0(y) = \begin{cases} 3\tanh^2\left[\left(\dfrac{\beta}{2\epsilon}\right)^{1/2} y + \tanh^{-1}\left(\dfrac{\psi+2}{3}\right)^{1/2}\right] - 2 & \text{if} \quad 0 \le y \le 1, \\ 3\phi\coth^2\left[-\left(\dfrac{\beta}{2\epsilon\phi}\right)^{1/2} y + \coth^{-1}\left(\dfrac{\psi+2\phi}{3\phi}\right)^{1/2}\right] - 2\phi & \text{if} \quad -B_v \le y \le 0. \end{cases} \tag{24}$$

The streamwise velocity in the base state U_0 is found to be expressed by hyperbolic-tangent and hyperbolic-cotangent functions which are invariant in time and in the streamwise direction and include four non-dimensional parameters, β, ϵ, ψ and ϕ, where the later two can be expressed as functions of only α.

Figs. 3(a), (b) and (c) depict the lateral distribution of U_0 as in (24) as functions of the parameters β, ϵ and α, respectively. Note that the velocities at the far right and left correspond to $\tilde{U}_\infty$ and $\tilde{U}_{-\infty}$, and the value of U_0 at the far left is ϕ. It is found from Fig. 3(a) that, as β increases, the width of the shear layer decreases. This is because an increase in β implies an increase in the relative significance of the bed friction over the vegetation drag. In Fig. 3(b), on the other side, the increase of ϵ results in the increase of the shear layer width following the increase of the relative importance of the sub-depth kinematic eddy viscosity. The relative increase of the viscous effects will result in a milder lateral gradient of the base state velocity. According to Fig. 3(c), ϕ decreases with increasing α, as it is natural that the velocity difference between the two zones increases with the vegetation drag parameter. In contrast to β and ϵ, the shear layer width does not strongly depend on α.

LINEAR STABILITY ANALYSIS

A temporal linear stability analysis is performed herein. A disturbance undulating in the streamwise direction is introduced to the base state. The streamwise and lateral velocities U and V, and the flow depth H are then expanded in the form

$$U(x,y,t) = U_0(y) + AU_1(y)\mathrm{e}^{\mathrm{i}(kx-\omega t)}, \tag{25a}$$

$$V(x,y,t) = AV_1(y)\mathrm{e}^{\mathrm{i}(kx-\omega t)}, \tag{25b}$$

$$H(x,y,t) = 1 + AH_1(y)\mathrm{e}^{\mathrm{i}(kx-\omega t)}, \tag{25c}$$

where A, k and ω are the amplitude, wavenumber and angular frequency of perturbation. In the scheme of temporal linear stability analysis, k is real while ω is complex such that $\omega = \omega_r + i\Omega$, where ω_r is the real angular frequency and Ω is the growth rate of perturbation.

Substituting (25) into the governing equations (14), we obtain the following perturbed equations in the non-vegetated zone:

$$\left[\mathrm{i}\left(kU_0-\omega\right)+k^2\epsilon+2\beta U_0-\epsilon\frac{\mathrm{d}^2}{\mathrm{d}y^2}\right]U_1+\frac{\mathrm{d}U_0}{\mathrm{d}y}V_1+\left(\mathrm{i}kF^{-2}-\beta U_0^2\right)H_1 = 0, \tag{26a}$$

$$\left[\mathrm{i}\left(kU_0-\omega\right)+k^2\epsilon+\beta U_0-\epsilon\frac{\mathrm{d}^2}{\mathrm{d}y^2}\right]V_1+F^{-2}\frac{\mathrm{d}H_1}{\mathrm{d}y} = 0, \tag{26b}$$

$$\mathrm{i}kU_1+\frac{\mathrm{d}V_1}{\mathrm{d}y}-\mathrm{i}(\omega-kU_0)H_1 = 0. \tag{26c}$$

In the vegetated zone, (14) reduces to

$$\left[\mathrm{i}\left(kU_0-\omega\right)+k^2\epsilon+2\beta U_0\left(1+\alpha\right)-\epsilon\frac{\mathrm{d}^2}{\mathrm{d}y^2}\right]U_1+\frac{\mathrm{d}U_0}{\mathrm{d}y}V_1+\left(\mathrm{i}kF^{-2}-\beta U_0^2\right)H_1 = 0 \tag{27a}$$

$$\left[\mathrm{i}\left(kU_0-\omega\right)+k^2\epsilon+\beta U_0\left(1+\alpha\right)-\epsilon\frac{\mathrm{d}^2}{\mathrm{d}y^2}\right]V_1+F^{-2}\frac{\mathrm{d}H_1}{\mathrm{d}y} = 0 \tag{27b}$$

$$\mathrm{i}kU_1+\frac{\mathrm{d}V_1}{\mathrm{d}y}-\mathrm{i}\left(\omega-kU_0\right)H_1 = 0 \tag{27c}$$

Since the amplitude of the perturbation A is assumed to be infinitesimally small, the terms containing A^2 have been dropped in the linear stability analysis, so that the results of the analysis are valid only in the range of small amplitudes.

The boundary conditions of vanishing lateral velocity (7b) and vanishing shear stress (8) at the side walls take the following forms at $O(A)$:

$$\frac{\partial U_1}{\partial y} = 0 \qquad \text{at} \qquad y = -B_v, 1, \tag{28a}$$

$$V_1 = 0 \qquad \text{at} \qquad y = -B_v, 1. \tag{28b}$$

At the interface between the vegetated and non-vegetated zones $y = 0$, the matching conditions reduce to

$$\lim_{y \to +0} \left(U_1, V_1, H_1, \frac{\partial U_1}{\partial y}, \frac{\partial V_1}{\partial y} \right) = \lim_{y \to -0} \left(U_1, V_1, H_1, \frac{\partial U_1}{\partial y}, \frac{\partial V_1}{\partial y} \right). \tag{29}$$

Although there are five matching conditions in (29), only four of them are independent since, if four of them are imposed, the other condition is automatically satisfied. Thus, one of these conditions can be dropped afterwards.

A numerical scheme is necessary to solve (26) and (27) under the boundary and matching conditions (28) and (29), as the equations obviously do not admit analytical solutions. We employ a spectral collocation method with the Chebyshev polynomials. In the non-vegetated zone ($0 \leq y \leq 1$), the variables U_1, V_1 and H_1 are expanded in the form

$$U_1 = \sum_{j=0}^{N} a_j T_j(\xi), \quad V_1 = \sum_{j=0}^{N} a_{(N+1)+j} T_j(\xi), \quad H_1 = \sum_{j=0}^{N} a_{2(N+1)+j} T_j(\xi), \tag{30}$$

and, in the vegetated zone ($-B_v \leq y \leq 0$), they are expanded in the form

$$U_1 = \sum_{j=0}^{N} a_{3(N+1)+j} T_j \left(\zeta\right), \quad V_1 = \sum_{j=0}^{N} a_{4(N+1)+j} T_j \left(\zeta\right), \quad H_1 = \sum_{j=0}^{N} a_{5(N+1)+j} T_j \left(\zeta\right), \tag{31}$$

where a_j ($j = 0, 1, 2, ..., 6N + 5$) are the coefficients of the Chebyshev polynomials, and $T_j(\xi)$ and $T_j(\zeta)$ are the Chebyshev polynomials in ξ and ζ of degree j. The independent variables ξ and ζ both range from -1 to 1, and are related to y by the equations $\xi = 2y - 1$ ($0 \leq y \leq 1$) and $\zeta = 2y/B_v + 1$ ($-B_v \leq y \leq 0$), respectively. The expansions (30) and (31) are substituted into the governing equations (26) and (27) respectively, and the resulting six equations are evaluated at the Gauss-Lobatto points, defined by

$$\xi_m = \cos\frac{m\pi}{N}, \quad \zeta_m = \cos\frac{m\pi}{N}, \tag{32}$$

where $m = 0, 1, ..., N$. Therefore, the number of points where the governing equations are evaluated is $N + 1$. We obtain a system of $6(N + 1)$ algebraic equations with $6(N + 1)$ unknown coefficients $a_0, a_1, a_2, ..., a_{6N+5}$. Eight equations of the system are then replaced by the four boundary conditions (28) and four of the matching conditions (29). The resulting linear algebraic system can be written in the form

$$\mathcal{M} \begin{bmatrix} a_0 & a_1 & \dots & a_{6N+5} \end{bmatrix}^T = 0, \tag{33}$$

where $\mathcal{M}$ is a $6(N+1) \times 6(N+1)$ matrix in which the elements consist of the coefficients of U_1, V_1 and H_1 in the governing equations (26) and (27), and the boundary and matching conditions (28) and (29). The condition for (33) to have a non-trivial solution is that $\mathcal{M}$ should be singular. Thus,

$$|\mathcal{M}| = 0. \tag{34}$$

The solution of the above equation takes the functional form

$$\omega = \omega\left(k, \beta, \epsilon, \alpha, B_v, F\right). \tag{35}$$

RESULTS AND DISCUSSION

As seen in (35), there are six important non-dimensional parameters k, β, ϵ, α, B_v, and F determining the growth rate Ω. The contours of the growth rate Ω on the plane of these parameters are shown in Figs. 4–8. When Ω is positive, the perturbations grow with time, whereas the perturbations decay until they vanish when Ω is negative. The thick solid lines in the figures indicate the neutral instability curve on which $\Omega = 0$ and the perturbations neither grow nor decay, and divide the planes into stable ($\Omega < 0$) and unstable regions ($\Omega > 0$). In the figures, Ω typically becomes negative in the range of sufficiently small and large values of k, and takes a maximum value between them. It follows that Ω as a function of k commonly possesses a characteristic wavenumber

k_m associated with the maximum growth rate Ω_m, implying the selection of a preferential wavelength at the linear level.

The parameters β, ϵ, α, B_v, and F were systematically varied from a base set of numerical values consisting of $\beta = 0.05$, $\epsilon = 6 \times 10^{-4}$, $\alpha = 10$, $B_v = 0.55$ and $F = 0.5$. These values were defined based on typical values of the experiments of Ikeda et al. (1991). $N = 30$ was adopted in the Chebyshev polynomials, with results independent of the numerical resolution.

In Fig. 4(a), the dependence of Ω on β is studied for the case $\epsilon = 6 \times 10^{-4}$, $\alpha = 10$, $B_v = 0.55$ and $F = 0.5$, following the base set of values for these parameters. The growth rate Ω is maximized when β is around 10^{-1}. As β increases or decreases from this value, the flow becomes less stable, and in the range $\beta \gtrapprox 0.5$, the region of positive Ω completely disappears and the flow becomes stable. In the range of large β, the effect of the bottom friction inhibits the effect of the lateral velocity gradient, as already shown by Chu et al. (1991) and White and Nepf (2007). On the other side, in the range of small β, the relative effect of the small scale turbulences generated by the bottom friction will be reduced, allowing the shear layer to expand further along the transverse direction and leading to a milder lateral gradient of the base state velocity, as in Fig. 3(a), leading to the reduction of the growth rate Ω. Although the present shallow water formulation may no longer be valid in the range of $\beta \lessapprox 5 \times 10^{-3}$, the decrease in the growth rate Ω is expected to occur in this range. In the range of sufficiently small β, the shear layer may be affected by the zero disturbance boundary condition of the walls, as pointed by Kolyshkin and Ghidaoui (2002). The range of k for positive Ω and the characteristic wavenumber k_m increase with β. This is because the wavenumber k is normalized by the width of the non-vegetated zone $\tilde{B}$.

The effect of the parameter ϵ on Ω is studied in Fig. 5. The parameter ϵ measures the relative effect of the sub-depth kinematic eddy viscosity. Because the sub-depth kinematic eddy viscosity is derived taking into consideration the small scale turbulences generated by the bottom friction before instability takes place, ϵ does not contain the effect of the large-scale turbulences. It is found from Fig. 5 that the flow becomes stable when $\epsilon \gtrapprox 4.0 \times 10^{-3}$. In this range, the dissipation of energy caused by the small scale turbulences will be sufficiently large to suppress the effect of the transverse mixing. On the other side, as ϵ decreases, Ω increases. In the range of very small ϵ, the flow approaches to the inviscid case. The characteristic wavenumber k_m increases with the decrease of ϵ because of the normalization of the wavenumber k. If we had employed the kinematic eddy viscosity as in Chen and Jirka (1997), the growth rate of perturbations would have been underestimated, following that a larger eddy viscosity would correspond to a smaller growth rate Ω.

The dependence of Ω on the vegetation drag parameter α is studied in Fig. 6. It is found that, in the range of small α, Ω is negative and the flow is stable as already pointed out by Chu et al. (1991) and White and Nepf (2007). As α increases, Ω increases with a slight increase in k_m, which peaks around the point $(\alpha, k) \approx (10^2, 6)$. In the range of $\alpha \gtrapprox 10^2$, Ω decreases with a slight decrease in k_m, and Ω becomes negative and the flow becomes stable again when $\alpha \gtrapprox 4 \times 10^3$. In the present analysis, we assume that the kinematic eddy viscosity in the vegetated zone is represented by (6) since the typical length scale of vegetation is not significantly smaller than the flow depth. When the vegetation density reaches a certain density, this assumption may no longer be valid. However, it is natural that the flow becomes stable with increasing α since the vegetated zone becomes like a cavity region when α is sufficiently large, and the large-scale horizontal vortices are damped by strong retardation effects. Therefore, the contours of Ω in the range of large α in Fig. 6 are at least qualitatively correct.

The effect of the width of the vegetated zone B_v on Ω is shown in Fig. 7. It is found from the figure that Ω is negative for any value of k when $B_v \lessapprox 0.1$, and Ω is almost independent of B_v when $B_v \gtrapprox 0.5$. In this analysis, we assume that B_v is large enough that U_0 is almost constant at $y = -B_v$ as described in (9). Therefore, Fig. 7 is not reliable in the range of small B_v. However, Fig. 7 is at least qualitatively correct because the lateral displacement of water is suppressed and the flow becomes stable when B_v is sufficiently small.

The dependence of Ω on the Froude number F is studied in Fig. 8. Because the rigid-lid assumption was not employed in the present analysis, the growth rate of perturbations can also be studied for values of F which are not close to zero. It is found from the figure that the flow is unstable in the range of small F. As F increases, the instability weakens and a stable region is observed in the range $F \approx 2.3 - 2.6$. When $F \gtrapprox 2.6$ under the conditions of this figure, the flow is again found to be unstable. It has been empirically known that rapid flow plays stabilizing effects for lateral velocity gradients, which is theoretically explained in this analysis. On the other side, as pointed by Kolyshkin and Ghidaoui (2002), the rapid flow becomes unstable to gravity waves if F is sufficiently large. Therefore, although the flow is found to be stable to the lateral velocity gradients when $F \gtrapprox 2.3$ in Fig. 8, it is unstable to gravity when $F \gtrapprox 2.6$. Fig. 9 depicts the neutral instability curves ($\Omega = 0$) for the case $\beta = 0.05$, $\epsilon = 6 \times 10^{-4}$, and $B_v = 0.55$ for varying α and multiple Froude numbers F. While the flow is stable when $\alpha \lessapprox 0.5$ for $F = 0.5$ and $F = 1.5$, it becomes unstable to gravity in this range when $F = 2.5$. As F increases from 0.5 to 2.5, the unstable region for $\alpha \gtrapprox 0.5$ diminishes because the gravity effects weaken the instability due to the transverse mixing. The combined effect of rapid flow and lateral mixing stabilizes the flow in the range of $\alpha \approx 10^1$ for $F = 2.5$.

Once the characteristic frequency of the generation of vortices ω_{rm} associated with the maximum growth rate Ω_m is determined, the corresponding time period $\tilde{T}$ can be calculated by the following relation:

$$\tilde{T} = \frac{2\pi \tilde{B}}{\omega_{rm} \tilde{U}_n}. \tag{36}$$

Assuming that the perturbation with the maximum growth rate Ω_m is realized in experiments and in the field, we compare $\tilde{T}$ predicted in the analysis with the results of the laboratory experiments obtained by Ikeda et al. (1994) and Tsujimoto (1991). In their experiments, vortices were generated by an array of regularly spaced cylinders installed on one side of channels, which is the same setup as assumed in the present analysis. The major hydraulic parameters of the experiments are listed in Table 1.

Fig. 10 depicts a comparison between the predicted and measured values of the period of generation of vortices $\tilde{T}$. In the figure, the crosses correspond to the results obtained with the use of (6), and the closed circles correspond to the results obtained with the use of the eddy viscosity proposed by Chen and Jirka (1997). For the sub-depth eddy viscosity $\tilde{\nu}_T$ from (6), the predictions are generally smaller than the observations by a factor of approximately two. Ikeda et al. (1994) made a comparison between the vortex shedding periods observed in their experiments and those predicted by their linear stability analysis, and showed good agreement between them. Their analysis employed the lateral kinematic eddy viscosity observed in their experiments which is approximately twice as large as in (6). Similarly, we performed a linear stability analysis of the experimental cases of Table 1 employing the eddy viscosity of Chen and Jirka (1997) and the agreement was better in comparison with the results corresponding to the eddy viscosity from (6), as depicted in Fig. 10.

The vortex shedding periods observed in the experiments correspond to a fully developed stage, while the results of the linear analysis can reliably reflect only an initial stage of the growth of infinitesimally small disturbances. Although the use of an increased eddy viscosity in the linear analysis led to a good estimation of the vortex shedding periods, this is because the nonlinear interactions may result in the increase of the mixing efficiency, which is apparently equivalent to the increase in the kinematic eddy viscosity.

The vortex shedding period may be longer due to the nonlinear interaction among vortices with a variety of length scales and frequencies. Therefore, in order to gain a qualitative understanding of the effect of nonlinear interaction, a weakly nonlinear stability analysis will no doubt prove useful.

CONCLUSIONS

In this paper, we propose a new linear stability analysis of flow with a lateral velocity gradient due to the presence of vegetation on one side of an open channel. In the analysis, we employ the St. Venant shallow water equations, and include the Reynolds stresses represented by the kinematic eddy viscosity, which characterizes the sub-depth scale turbulence generated by the bottom friction. In the base state, the velocity distributions inside and outside vegetation are expressed by hyperbolic cotangent and hyperbolic tangent functions squared respectively. These functions are determined analytically, by considering as the base state not the average flow, but the flow without the effects of the large-scale horizontal vortices.

We performed a temporal linear stability analysis by imposing small perturbations on the base state flow velocities and depth. We obtained a set of instability diagrams with respect to six non-dimensional parameters, including a kinematic eddy viscosity parameter, following that we did not employ a formulation for inviscid flow. Our results indicate that, while the base state flow field is unstable in the range of typical, moderate values of the hydraulic parameters, stability is retained in the range of sufficiently small and large vegetation densities, small widths of the vegetated zone, large bed shear effect, large sub-depth eddy viscosity effect, and moderate Froude numbers where the flow is stable to both the transverse mixing and the gravity. The growth rate of perturbations could be evaluated for Froude numbers far from zero because the rigid-lid assumption was not used. The use of a theoretical sub-depth kinematic eddy viscosity unaffected by the lateral motions permitted a consistent estimation of the growth rate of perturbations, as these perturbations were imposed to a base flow which is independent of the large-scale lateral motions. Assuming that the characteristic wavenumber and frequency of perturbations associated with maximum perturbation growth rate correspond to those of vortices realized in experiments, we compare predicted and observed vortex shedding frequencies. There is a systematic discrepancy in the frequencies predicted from employing a sub-depth eddy viscosity undisturbed by the vortices, when compared to the observed frequencies. This discrepancy, typically in the range of a factor of approximately two, may be caused by the limitation of linear stability analysis.

REFERENCES

Chen, D. and Jirka, G. H. (1997). “Absolute and convective instabilities of plane turbulent wakes in a shallow water layer.” *Journal of Fluid Mechanics*, 338, 157–172.

Chu, V. H., Wu, J.-H., and Khayat, R. E. (1991). “Stability of transverse shear flows in shallow open channels.” *Journal of Hydraulic Engineering, ASCE*, 117, 1370–1388.

Ghidaoui, M. S. and Kolyshkin, A. A. (1999). “Linear stability analysis of lateral motions in compound open channel.” *Journal of Hydraulic Engineering, ASCE*, 125, 871–880.

Ikeda, S., Izumi, N., and Itoh, R. (1991). “Effects of pile dikes on flow retardation and sediment transport.” *Journal of Hydraulic Engineering, ASCE*, 117(11), 1459–1478.

Ikeda, S., Ohta, K., and Hasegawa, H. (1994). “Instability-induced horizontal vortices in shallow open-channel flows with an inflection point in skewed velocity profile.” *Journal of Hydroscience and Hydraulic Engineering*, 12, 69–84.

Kolyshkin, A. A. and Ghidaoui, M. S. (2002). “Gravitational and shear instabilities in compound and composite channels.” *Journal of Hydraulic Engineering, ASCE*, 128, 1076–1086.

Michalke, A. (1964). “On the inviscid instability of hyperbolic tangent velocity profile.” *Journal of Fluid Mechanics*, 19, 543–556.

Prooijen, B. C. and Uijttewaal, W. S. J. (2002). “A linear approach for the evolution of coherent structures in shallow mixing layers.” *Physics of Fluids*, 14, 4105–4114.

Tamai, N., Asaeda, T., and Ikeda, H. (1986). “Study on generation of periodical large surface eddies in a composite channel flow." *Water Resources Research*, 22(7), 1129–1138.

Tsujimoto, T. (1991). "Open channel flow with bank vegetation." *KHL Communication*, 2, 41–54.

Tsujimoto, T. and Kitamura, T. (1992). "Experimental study on open-channel flow with vegetated zone along side wall." *KHL Progressive Report*, 29–35.

White, B. L. and Nepf, H. M. (2007). "Shear instability and coherent structures in shallow flow adjacent to a porous layer." *Journal of Fluid Mechanics*, 593, 1–32.

Xiaohui, S. and Li, C. W. (2002). "Large eddy simulation of free surface turbulent flow in partially vegetated open channels." *International Journal of Numerical Methods in Fluids*, 39, 919–937.

NOTATION

The following symbols are used in this paper:

$A =$ amplitude;

$A_R =$ aspect-ratio of the non-vegetated zone;

$a =$ vegetation density parameter;

$B =$ non-vegetated zone width;

$B_v =$ vegetated zone width;

$C_d =$ vegetation drag coefficient;

$C_f =$ bed friction coefficient;

$D_x, D_y =$ streamwise and transverse vegetation drag components, respectively;

$d =$ diameter of cylinders;

$F =$ Froude number;

$g =$ gravity acceleration;

$H =$ flow depth;

$k =$ wavenumber;

$l_x, l_y =$ distances between two adjacent cylinders in x and y directions;

$S =$ streamwise bed slope of the channel;

$T_{bx}, T_{by} =$ streamwise and transverse bed shear stress components, respectively;

$T_{i,j}$ $(i, j = x, y) =$ Reynolds stress tensor;

$T_j(\xi), T_j(\zeta) =$ Chebyshev polynomials in ξ and ζ of degree j;

$t =$ time;

$U, V =$ streamwise and transverse velocities, respectively;

$U_0 =$ base state flow velocity;

$U_1, V_1, H_1 =$ eigenfunctions;

$U_f =$ friction velocity;

$x, y =$ streamwise and transverse coordinates, respectively;

$\alpha =$ vegetation drag parameter;

$\beta =$ bed friction parameter;

$\epsilon =$ sub-depth eddy viscosity parameter;

$\kappa =$ Kármán constant;

$\nu_T =$ kinematic eddy viscosity;

$\rho =$ water density;

$\phi =$ ratio between the undisturbed velocities in the vegetated zone and the non-vegetated zone;

$\psi =$ base state flow velocity at the interface between the non-vegetated and vegetated zones;

$\omega = \omega_r + i\Omega =$ angular frequency.

Subscripts:

$\infty, -\infty =$ far field in the non-vegetated and vegetated zones, respectively;

$m =$ most unstable mode.

List of Tables

TABLE 1. Hydraulic parameters in Ikeda et al.'s (1994), run 1–5, and Tsujimoto's (1991), run IW1–IW3.

Run	β	ϵ ($\times 10^{-4}$)	α	B_V	F	Measured $\tilde{T}$(s)
1	0.060	5.02	10.2	0.57	0.41	6.4
2	0.061	5.07	10.0	0.57	0.75	3.8
5	0.025	5.48	17.2	0.57	0.44	9.0
IW1	0.024	4.84	67.7	0.43	0.69	3.3
IW2	0.030	5.84	51.0	0.43	0.78	2.5
IW3	0.025	5.40	61.2	0.43	0.93	1.9

List of Figures

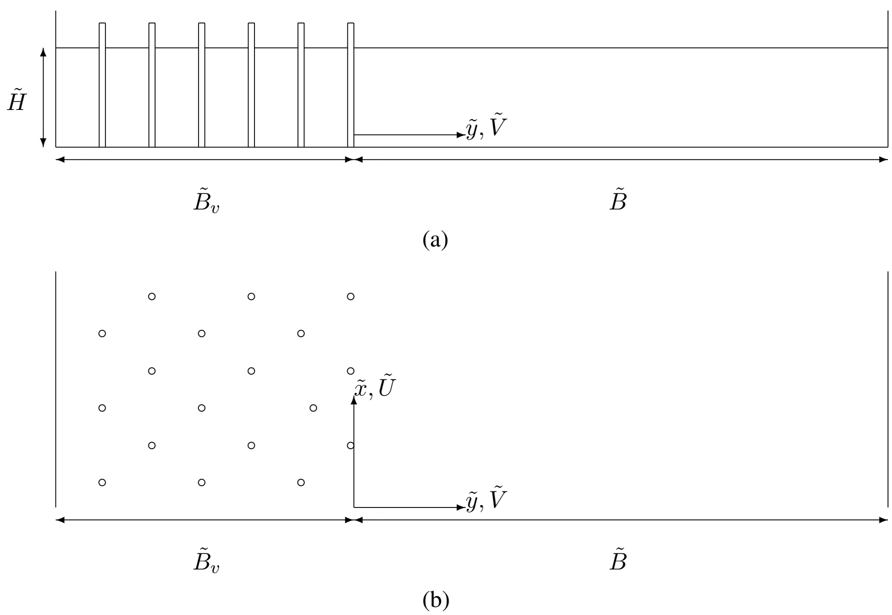

FIG. 1. Conceptual diagram of the channel with vegetation. (a) The cross-sectional view, and (b) the plan view.

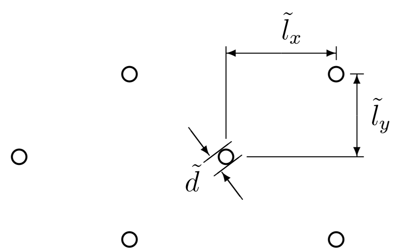

FIG. 2. The plan view of an array of regularly-spaced cylinders as a model of vegetation.

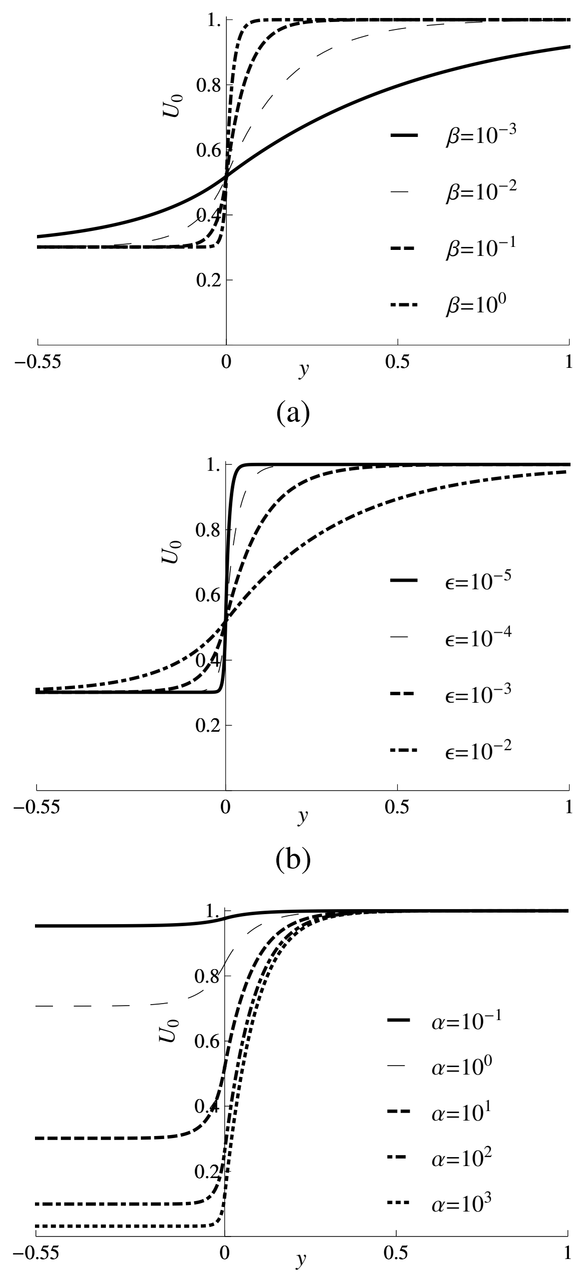

(c)

FIG. 3. The lateral distribution of the streamwise velocity in the base state U_0 as functions of (a) β for the case $\epsilon = 6 \times 10^{-4}$, $\alpha = 10$, (b) ϵ for the case $\beta = 0.05$, $\alpha = 10$, and (c) α for the case $\beta = 0.05$, $\epsilon = 6 \times 10^{-4}$.

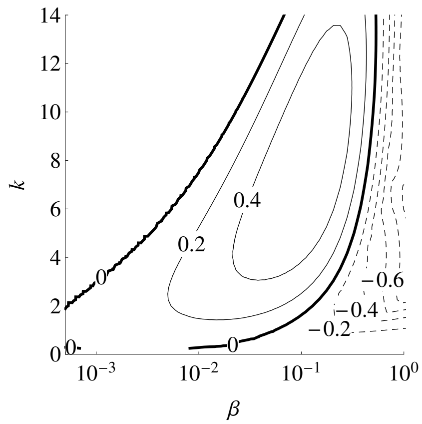

FIG. 4. The contours of the perturbation growth rate Ω in the β-k plane for the case $\epsilon = 6 \times 10^{-4}$, $\alpha = 10$, $B_v = 0.55$, $F = 0.5$.

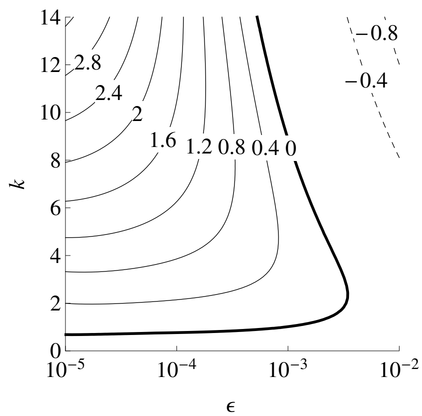

FIG. 5. The contours of the perturbation growth rate Ω in the ϵ-k plane for the case $\beta = 0.05$, $\alpha = 10$, $B_v = 0.55$, $F = 0.5$.

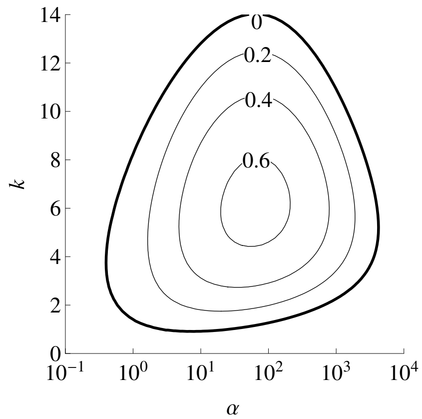

FIG. 6. The contours of the perturbation growth rate Ω in the α-k plane for the case $\beta = 0.05$, $\epsilon = 6 \times 10^{-4}$, $B_v = 0.55$, $F = 0.5$.

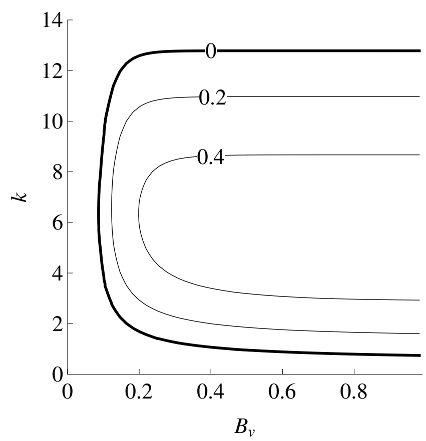

FIG. 7. The contours of the perturbation growth rate Ω in the B_v-k plane for the case $\beta = 0.05$, $\epsilon = 6 \times 10^{-4}$, $\alpha = 10$, $F = 0.5$.

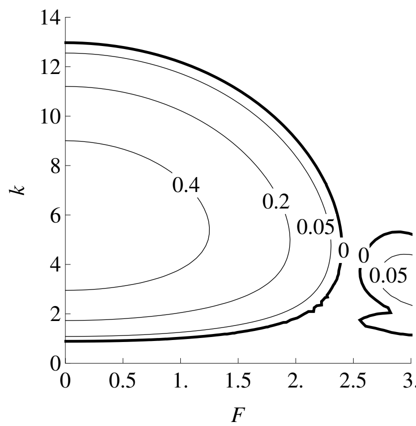

FIG. 8. The contours of the perturbation growth rate Ω in the F-k plane for the case $\beta = 0.05$, $\epsilon = 6 \times 10^{-4}$, $\alpha = 10$, $B_v = 0.55$.

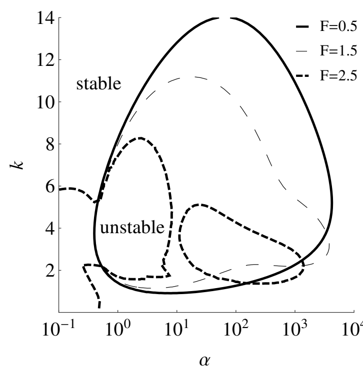

FIG. 9. The contours of the neutral instability ($\Omega = 0$) in the α-k plane for the case $\beta = 0.05$, $\epsilon = 6 \times 10^{-4}$, $B_v = 0.55$ and multiple Froude numbers F.

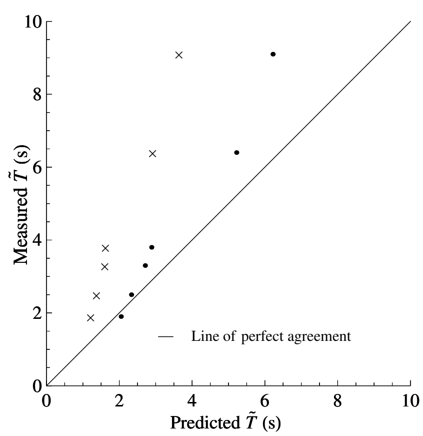

FIG. 10. Comparison between the predicted and measured periods of generation of vortices $\tilde{T}$ ($\times$: eddy viscosity from (6); $\bullet$: eddy viscosity from Chen and Jirka (1997)).